Small strain behavior of sand under various stress paths considering anisotropic initial stress state

Lai Yong[1], Shi Jian-yong[1], Yu Xiao-jun[1] and Cao Qiu-rong[1]
[1]*Geotechnical Engineering Research Institute, Hohai University, Nanjing, China*
E-mail: soft-ground@hhu.edu.cn

ABSTRACT: The stress-strain characteristics in small strain region for a Chinese sand were investigated under different stress paths. The strain contour circle method was used to simulate the small strain characteristics of the sand under various stress paths. The test results showed that the inherent stress-strain characteristics of the sand depend on the anisotropic initial stress state. The contraction and dilation behaviors of the tested sand under various K_0 initial stress conditions are different from that under isotropic initial stress state conditions. The test results of the sand agreed with the Wong-Mitchell's research results very well. The strain contour circle method can approximately simulate small stress-strain characteristics of the sand for various stress paths by using the proportion function λ and expansion function l. The calculation results from the new method agree with the test results for Bothkennar clay.

Keywords: small strain behavior, anisotropic initial stress state, stress path, strain contour circle method, bounding surface

1. INTRODUCTION

The stress path is very complex in earth structures. For example, mean stress and shear stress at one point increase when constructing a dam and a dike, but mean stress decreases and shear stress increases during excavation. The strain of soil caused by load is normally small, which is approximately between 0.05% and 0.1% in foundation and underground engineering (Burland, 1989). Many studies have been conducted on small strain behavior of clay (Jardine *et al*., 1984; Clayton & Khatrush, 1989; Atkinson *et al.*, 1990; Thomann & Hryciw, 1990; Simpson, 1992; Viggiani & Atkinson, 1995; Goto *et al*., 1999; Lings *et al*., 2000; Clayton & Heymann, 2001; Gasparre *et al*., 2007; Hight *et al*., 2007; Clayton, 2011; Kim and Finno, 2012). The characteristics of sand and soft rock under small strain condition also drew attention (Jardine *et al*.,1985; Jardine, 1992). In existing soil test or constitutive model on small strain, numerous studies on nonlinear stress–strain relationship and stress path–dependency have been conducted (Shibuya *et al*., 1992; Smith *et al*., 1992; Lo Presti *et al*., 1997; Goto *et al*., 1997; Charles *et al*., 2000; Clayton & Heymann, 2001; Kim and Finno, 2012). The Bothkennar clay was firstly consolidated to in-situ stress under K_0 condition. Then nine different test directions of stress paths were performed. Furthermore, the bounding surface shape and kinematic hardening rule of Bothkennar clay are presented in Smith *et al* (1992). Clayton & Heymann (2001) showed that the relationships between elastic modulus and strain acquired along two different current stress paths are prominently different, and the elastic modulus reduction with strain is different. Regarding constitutive modeling of small strain behavior, models of logarithmic and sinusoidal function mode were proposed, in which the deformation characteristics in small strain condition are reflected (Puzrin & Burland , 1998; Goto *et al* 1999). A model with three bounding surfaces and eight model parameters was proposed to simulate over consolidation and kinematic hardening in small strain region under different paths (Stallebrass & Taylor, 1997). The results were confirmed through centrifugal model test of circular foundation. On the basis of energy integral, a modified Cam-Clay model was presented under the condition of K_0 consolidation and small strain (Shi *et al*, 2001). The results were verified through typical stress path controlled triaxial test results.

In excavation and subway engineering, the behaviour of soil in small strain region is very important for deformation prediction and safety evaluation. There are many results of conventional triaxial tests and special stress path tests to simulate stress–strain relationship in scope of small strain. The stress–strain curves under various stress paths for clay are also presented before. However, the test results for sand are limited. It is necessary to modify the constitutive model under various stress paths.

The objective of this paper is developing test for the Chinese sand and conducting stress–strain relationship under various stress paths.

2. TEST MATERIAL AND METHOD

2.1 Specimens preparation

The sand is from Fujian Province in China. The main physical properties of the sand are shown in Table 1.

Table 1 Physical properties of the tested sand

Dry density (g/cm^3)	1.65
Specific gravity	2.67
Void ratio	0.618
Relative density	0.63
Particle size (mm)	0.5～1
Coefficient of permeability (cm/s)	1.43×10^{-2}

Specimens of the reconstituted Chinese sand are tested. The friction angle of the sand φ, obtained from conventional triaxial consolidated drained (CD) test, is 36°. The dry density of the specimens is controlled as 1.65g/cm^3. The height and diameter of test specimens are 80 mm and 38 mm, respectively. Firstly, the sand samples were mixed with de-aired water, boiled through sand bath, then cooled before specimen installation.

The test instrument is a standard triaxial stress path apparatus manufactured by GDS Company in UK. For specimen installation, firstly, sand and water were mixed evenly in a bowl. Then the mixture was put into a split mould in 9 portions and each portion of mixture was compacted lightly twice.

The small strain was measured by a Hall effect sensor (Clayton & Khatrush, 1989). Before installation of the sensor, a negative pressure of 4 kPa was applied on the specimen to ensure stability of specimen during installation. A special glue was used to seal the needle of Hall effect sensor and rubber membrane quickly and was applied on the rubber membrane within approximately half of specimen height from the middle section of specimen. Then the glue was smeared on the thrusting needles of Hall effect sensor, and the needles were pushed lightly into the specimen. The other parts of Hall effect sensor were installed 10 minutes later.

2.2 Stress path tests

The K_0 value of the sand, obtained from consolidation test under zero lateral strain, is 0.37. Before shear test, all specimens were consolidated along K_0 line to p'=150kPa and q=162.93kPa. After consolidation the drained shear tests were conducted under a stress control mode at a stress increment rate of 0.5 kPa / min. (Sultan et al,2010).The eight directions of the stress path are shown in Figure 1.

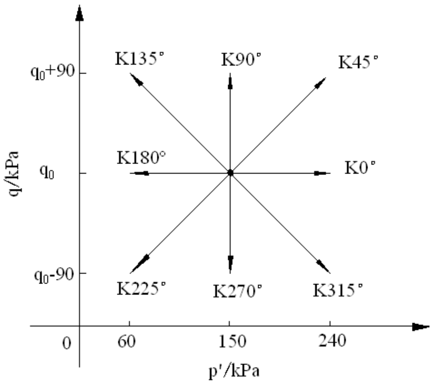

Figure 1 Stress path diagram

The stress path was controlled by the change of or/and to 90kPA

The stress path was controlled by the change of $\Delta p'$ or/and Δq to 90 kPa. The test time of each stress path is 3 hours. During shear tests, the changes of horizontal and vertical stresses are shown in Table 2.

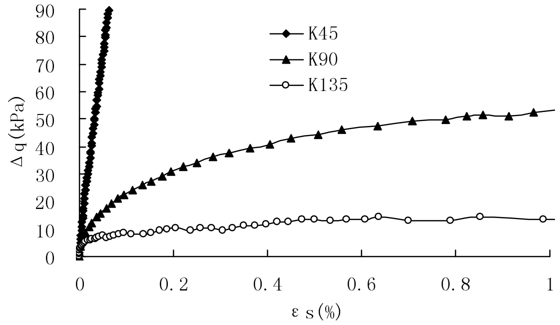

(a) Δq versus ε_s for positive Δq

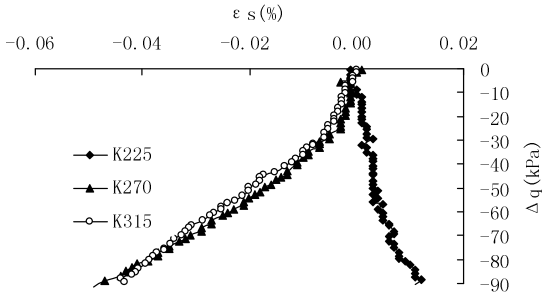

(b) Δq versus ε_s for negative Δq

Figure 2 Relationship between deviatoric stress and shearing strain

3. TEST RESULTS AND DISCUSSION

3.1 Relationship between deviatoric stress and shearing strain

When deviatoric stress increment Δq is positive, the specimens for stress path K90° and K135° fail before reaching the corresponding target deviatoric stress increment, i.e., 90kPa. The stress- strain relationship for shearing strain ε_s within 1% can be obtained in test and it is already met for small strain research. When Δq is negative, the shearing strain ε_s of the specimen is approximately -0.06%, the test results of Δq versus ε_s are shown in Figure 2(a) and (b) respectively.

In Figure 2(a), Δq of the stress path K45°, K90° and K135° are 90kPa, and $\Delta p'$ are 90kPa, 0kPa and -90kPa respectively. As shown in K90° test results with zero $\Delta p'$, ε_s increases with increasing Δq. By comparing with zero $\Delta p'$, it can be seen that ε_s decreases when $\Delta p'$ is positive.

In Figure 2 (b), the final Δq of stress path K225°, K270° and K315° are -90kPa, $\Delta p'$ are 90kPa, 0kPa and -90kPa respectively. Similarly, ε_s increases with increasing of Δq. By comparison with zero $\Delta p'$, ε_s decreases when $\Delta p'$ is positive.

Δq of stress path K0° and K180° are zero, and $\Delta p'$ is positive for stress path K0°. The results show that ε_s decreases. The value of $\Delta p'$ is negative for stress path K180°, and ε_s increases as shown in Figure 3. There are no changes for Δq of stress path of K0° and K180°. The increase in $\Delta p'$ causes the decrease in shear strain. The change of ε_s is not only related to Δq but is also affected by $\Delta p'$.

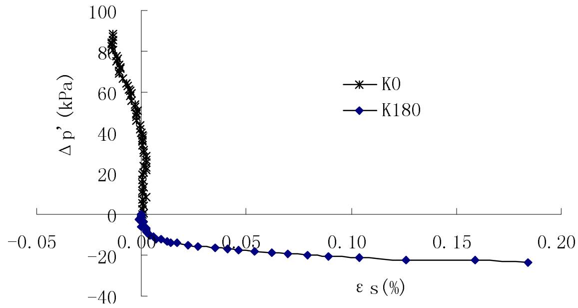

Figure 3 Relationship between mean stress and shearing strain

Table 2 Changes of horizontal and vertical stresses (kPa)

Stress path	K0°	K45°	K90°	K135°	K180°	K225°	K270°	K315°
Horizontal stress	90	150	60	-30	-90	-150	-60	30
Vertical stress	90	60	-30	-120	-90	-60	30	120

3.2 Relationship between mean stress and volumetric strain

The relationship between mean stress increment and volumetric strain is shown in Figure 4. The results indicate that ε_v is contraction when $\Delta p'$ increases. ε_v is dilation when $\Delta p'$ reduces.

Regarding the relationship between Δq and ε_v, the $\Delta p'$ of stress path K315°, K0° and K45° are all increased by 90kPa. The values of ε_v in the three specimens are all in contraction. Δq of stress path of K45° is increased by 90kPa, and Δq of stress path of K315° is reduced by 90kPa. Δq of K0° is 0, and ε_v is in contraction. The $\Delta p'$ of stress path of K135°, K180° and K225° are all reduced by 90kPa, and the values of ε_v of the three specimens are all in dilation. Δq of stress path K135° is increased by 90kPa. Δq of stress path K225° is reduced by 90kPa. Δq of stress path K180° is 0 and the values of ε_v are all in dilation. Volumetric strain ε_v is mainly subjected to effect of $\Delta p'$.

When the values of $\Delta p'$ of stress path K90° and K270° keep zero, the value of Δq of the stress path K90° increases and ε_v is dilative. While Δq of the stress path K270° decreases and ε_v is contractive. As shown in Figure 5, when $\Delta p'$ of stress path K90° and K270° remain unchanged, the increase of shear stress Δq leads to the dilation of volumetric strain ε_v. The stress-strain and volumetric relationships for the stress paths K45°, K135°, K225° and K 315° are shown in Figures 2 and 4, respectively. There is no normal shear contraction and dilatation for the stress path K90° and K270°, which results from anisotropic initial stress state before shear.

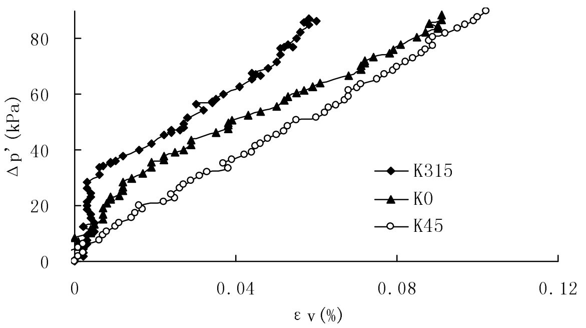

(a) $\Delta p'$ versus ε_v for positive $\Delta p'$

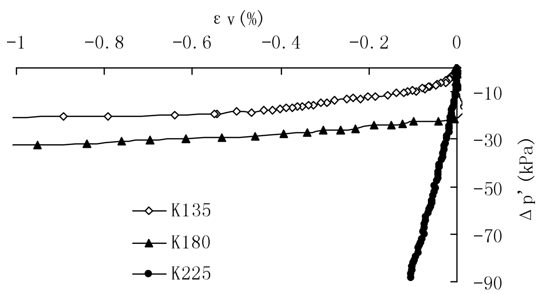

(b) $\Delta p'$ versus ε_v for negative $\Delta p'$

Figure 4 Relationship between mean stress and volumetric

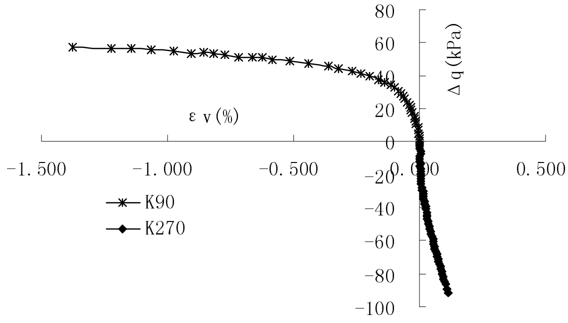

Figure 5 Relationship between deviatoric stress and volumetric strain

It is known that the direction of plastic strain is normal to bounding surface according to plastic mechanics. The bounding surfaces from Modified Cam-Clay model, Wong & Mitchell (1975) and Shi et al. (2001) are shown in Figure 6. When the K0° stress path reaches the bounding surface, the shear strain is negative and volumetric strain is contractive on the bounding surfaces of Wong-Mitchell and Shi. However, the shear strain is positive and volumetric strain is contractive on the bounding surfaces of Modified Cam-Clay model. From the test results of K0° stress path, the measured shear strain and volumetric strain (as shown in Figure 3 and Figure 4(a)) are identical with those on the bounding surfaces of Wong-Mitchell and Shi. Figure 6 also shows the other seven stress paths conducted in this study. Similar to K0° stress path, the measured shear strain and volumetric strain of these stress paths agree with those on the bounding surfaces of Wong-Mitchell and Shi.

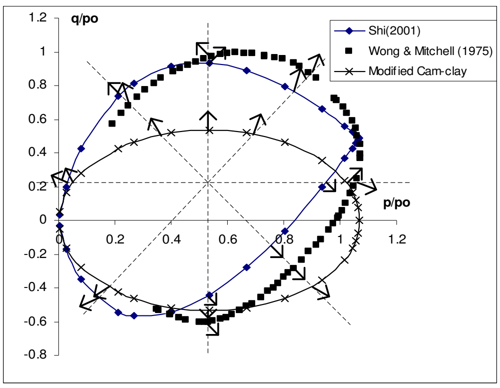

Figure 6 Relationship between plastic strain and bounding surface

The bounding surface of modified Cam-clay model is symmetrical, but the sand specimens of this study are under anisotropic initial stress state and the deformation is unsymmetrical. The test results are different from the modified Cam-clay model under the stress path K0°, K90° and K270°. The test results of the sand are identical with the unsymmetrical bounding surface proposed by Shi for seven stress paths (K0°, K45°, K135°, K180°, K225°, K270° and K315°). The only difference lies in the K90° stress path, and the bounding surface model proposed by Shi is almost consistent with the measured deformation characteristics of soil.

For stress paths K0°, K90°, K180° and K270°, the test results of Figures 3 and 5 can be explained by the unsymmetrical bounding surface of Wong-Mitchell and Shi in Figure 6. In Figure 3, $\Delta p'$ increases and Δq keeps constant (K0° stress path), the shear strain is negative. For the stress path K180°, $\Delta p'$ decreases and Δq keeps constant. The shear strain is positive, which is identical with the bounding surface of Wong-Mitchell and Shi. In Figure 5, Δq increases and $\Delta p'$ keeps constant (K90° stress path). The volumetric strain is dilative. For the stress path K270° it is only identical with the bounding surface of Wong-Mitchell, Δq decreases and $\Delta p'$ keeps constant, the volumetric strain is contractive, it can be identical with the bounding surface of Wong-Mitchell and Shi.

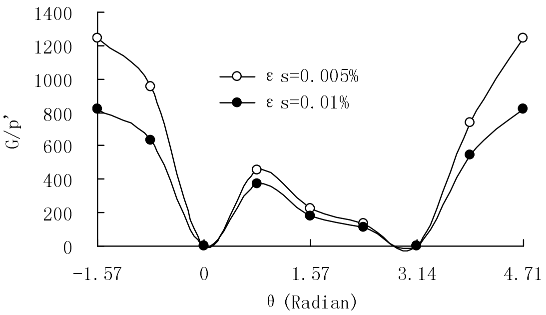

(a) Secant shear modulus and stress path

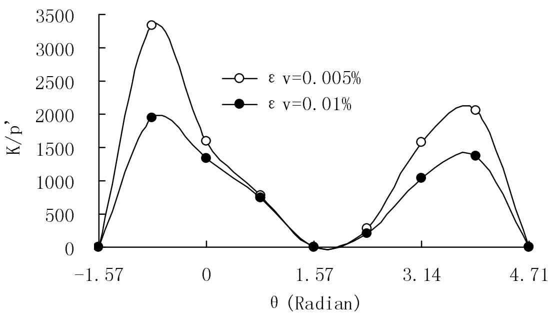

(b) Secant bulk modulus and stress path

Figure 7 Relationship between secant modulus and stress path

The relationship between shear and bulk modulus under different stress paths and strains are calculated and shown in Figure 7. The trend is similar with the shear modulus of Bothkennar clay (Smith et al, 1992) .

The results of the sand are identical with the bounding surface of Wong & Mitchell. It is indicated that the test results are credible.

3.3 Simulation of deformation characteristics in small strain range considering stress path

Jardine (1992) found that the small strain region of sandy soil is approximately 0.01%. In accordance with the results of stress path tests, the contour of axial strain less than 0.01% can be obtained, as shown in Figure 8.

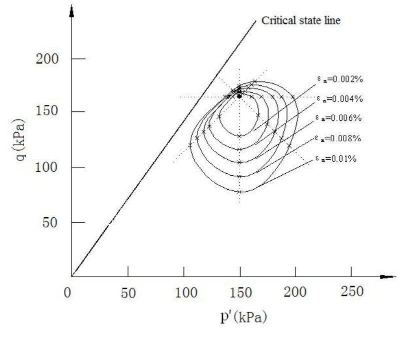

Figure 8 q-p curve of axial strain contour within 0.01% strain

Results in Figure 8 can be illustrated from three aspects: (1) The closer the strain contour is to critical state line, the smaller the distance between contour is, the smaller the stress gradient is, the smaller the elastic modulus is along the stress path direction due to the same strain increment. In direction parallel with the critical state line and apart from critical state line, the larger the stress gradient is, the larger the elastic modulus is. (2) The strain contour has similar circular shape under different strain values, which can be expressed with equation of the same mode; (3) With the increase in axial strain, the trace of contour center approaches a straight line. Therefore, it is assumed that the contour equation is circular, and is named as the strain contour circle. The strain contour circle center moves along a straight line. The choice of gradient of this line is to ensure that the strain contour is always expanding with increasing strain. The distance from the center to the critical state line is larger than the radius of strain contour circle. The slope is in the range from -1.0 to -5.0 and is adopted as $k_t = -\tan(45 + \varphi / 2)$ in small strain condition (Lai, 2005), which is shown in Figure 9.

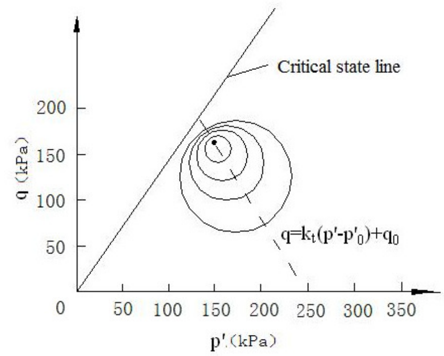

Figure 9 Diagram of simplified calculation of strain contour circle motion

Regarding the expansion of strain contour circle, in accordance with the test results presented in Jardine (1992), it can be drawn that the sum of Young's modulus of elasticity in compression and that in extension is approximately proportional to the mean stress when the extension and compression reach the same strain, for example, at axial strain 0.01%. The function $f(\varepsilon_a)$ is assumed to be constant under various stress paths at the same axial strain, and decreases with increasing axial strain.

$$\frac{E_{sc} + E_{se}}{p'_0} = f(\varepsilon_a) \tag{1}$$

where E_{sc} is the Young's modulus of elasticity in compression for given mean stress; E_{se} is the Young's modulus of elasticity in extension for the same mean stress; p'_0 is the mean stress at the stress point; $f(\varepsilon_a)$ is a function of axial strain ε_a, and is a constant corresponding to a given ε_a on different stress paths.

The relationships between Young's modulus of elasticity in compression/extension and mean stress are summarized in Table 3.

Table 3 shows that the Young's modulus of elasticity in compression and in tension, and their sum decreases with increasing axial strain.

$$q_c - q_e = p'_0 \cdot f(\varepsilon_a) \cdot \varepsilon_a = l \tag{2}$$

where q_c and q_e correspond to the deviatoric stress in compression and extension for an axial strain of ε_a. They are equivalent to OA and OB in Figure 10 and l is named as an expansion function.

Table 3 Change of Young's modulus of elasticity in different stress path directions

Axial strain	ε_a/%	0.002	0.004	0.006	0.008	0.01
Sample K90°	q_c/kPa	4	5	6	7	8
	E_c/MPa	200	125	100	88	80
Sample K270°	q_e/kPa	-33	-46	-60	-73	-88
	E_e/MPa	1650	1150	1000	913	880
$(E_c+E_e)/p'_0$		12333	8500	7333	6667	6400
$\varepsilon_a / ((E_c+E_e)/p'_0)$		1.6e-7	4.7e-7	8.2e-7	1.2e-6	1.6e-6
E_c/E_e		0.1212	0.1087	0.1000	0.0959	0.0909

$(E_{sc}+E_{se})/p'_0$ and ε_a can be expressed by a hyperbolic relationship as shown in Figure 11.

$$l = \frac{\varepsilon_a}{c_1 + c_2\varepsilon_a} \cdot p'_0 \cdot \varepsilon_a \tag{3}$$

where c_1 and c_2 are intercept and gradient of straight line in Figure 10, respectively. The best-fit values of c_1 and c_2 are 0.0 and 1.47×10^{-4} respectively.

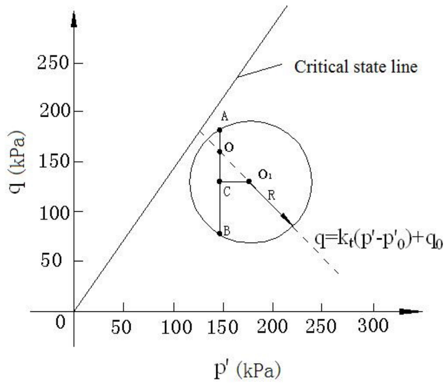

Figure 10 Calculation of strain contour circle equation and position

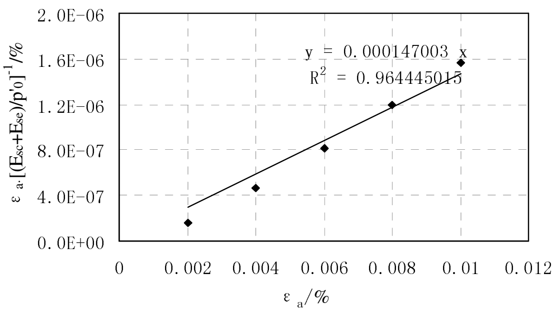

Figure 11 Relationship between $(E_{sc}+E_{se})/p'_0$ and ε_a

If the proportion of OA to OB corresponding to a certain stress can be determined, the strain contour circle can be determined uniquely. The proportion of OA to OB is actually the ratio of Young's modulus of elasticity in compression to that in extension for a mean stress of p'_0.

$$\lambda = \frac{OA}{OB} = \frac{q_c}{-q_e} = \frac{E_{sc}}{E_{se}} \tag{4}$$

The value of λ represents the change of Young's modulus of elasticity in compression and that in extension with respect to axial strain. The relationship between $\ln(E_{sc}/E_{se})$ and $\ln(\varepsilon_a)$ can be calculated and shown in Figure 12.

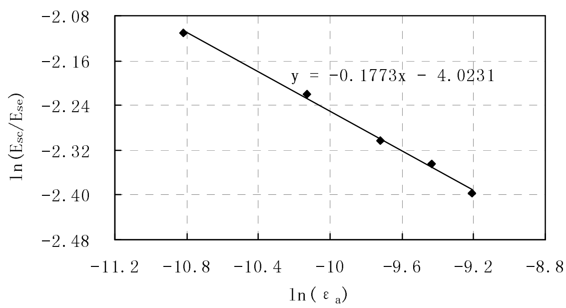

Figure 12 Relationship between E_{sc}/E_{se} and ε_a

Due to the fact that their relationship is approximate linearity in logarithm coordinates, the proportion function λ can be expressed as:

$$\lambda = a\varepsilon_a^{\ b} \tag{5}$$

where a and b are fitting coefficients. The best-fit values of a and b are 0.01789 and -0.1773, respectively.

The change in λ is not large with increasing axial strain within the small strain region ($\varepsilon_a < 0.01\%$). When the initial stress point is under compression state, the deviatoric stress is positive. The value of λ is usually less than 1 due to the fact that the elastic modulus in compression is smaller than that in extension. In the analysis, it can be taken as:

$$\lambda = 1 - M_0 / M_c \tag{6}$$

where $M_0 = q_0 / p'_0$, is the stress ratio of the initial consolidation line and M_c is the stress ratio of the critical state line, $M_c = 6\sin\phi'/(3-\sin\phi')$.

Therefore, the basic equation of strain contour circle is expressed as:

$$(q - c_y)^2 + (p' - c_x)^2 = R^2 \tag{7}$$

where c_x and c_y are co-ordinates of the center of circle, R is radius. The straight-line equation of circle center is:

$$c_y = k_t(c_x - p_0') + q_0 \tag{8}$$

where p_0' and q_0 are initial stresses.

In case of strain ε_a, the distance of circle center ordinate motion is calculated using Eq. (8). The geometrical relation according to Figure 9 is as following:

$$c_x = p'_0 - \frac{1-\lambda}{2k_t(1+\lambda)} l \tag{9}$$

According to the Eq. (9), change of circle radius R with axial strain using the geometrical relation is shown as following:

$$R = [\frac{(1-\lambda)^2 l^2}{4k_t^2(1+\lambda)^2} + \frac{l^2}{4}]^{1/2} \tag{10}$$

The comparison between the predicted strain contour circles and the measured values is presented in Figure 13. The characteristics of strain contour circle under different axial strains can be reflected.

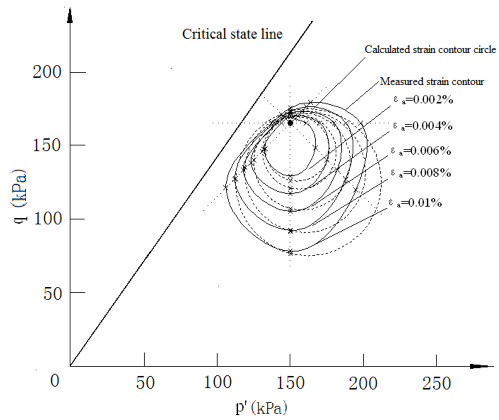

Figure 13 Comparison of strain contour circle from calculation and measurement

For a given strain ε_a and a direction of stress path that forms an angle θ with the p-axis, by combining Eqs. (3), (5) or (6) and (10), the increment in deviatoric stress Δq can be expressed as:

$$\Delta q(\theta) = \{(c_x - p'_0)(\cos\theta + k_t \sin\theta) + [R^2 - (c_x - p'_0)^2(\sin\theta - k_t\cos\theta)^2]^{1/2}\}\sin\theta \tag{11}$$

The parameters are listed in Table 4.

Table 4 Parameters in Eq. (11)

Parameters	c_1	c_2	A	B	φ(°)
Value	0.0	1.47×10^{-4}	0.01789	-0.1773	36

From Eq. (11) and strain ε_a in stress path direction that forms angle θ with axis p, the secant Young's modulus of elasticity along any stress path direction can be calculated by ratio of deviatoric stress with strain ε_a, it is seen as the following:

$$E_s(\theta) = \frac{\Delta q(\theta)}{\varepsilon_a} = \frac{l\sin\theta\{(\lambda-1)\cdot(\cos\theta + k_t\sin\theta) - [(1-\lambda)^2(\cos^2\theta - k_t^2\cos^2\theta + k_t\sin 2\theta) + k_t^2(1+\lambda)^2]^{1/2}\}}{2k_t\varepsilon_a(1+\lambda)} \tag{12}$$

Figure 14 shows a comparison between the predicted deviatoric stresses using Eq. (11) and the measured values under different directions of stress path and axial strains.

Figure 15 depicts the predicted secant Young's modulus of elasticity using Eq. (12) under different directions of stress path and axial strains.

Comparing Figures 14 and 15, it can be seen that Eqs. (11) and (12) can reflect the effects of small strain and stress path on the deviatoric stress and secant Young's modulus of elasticity.

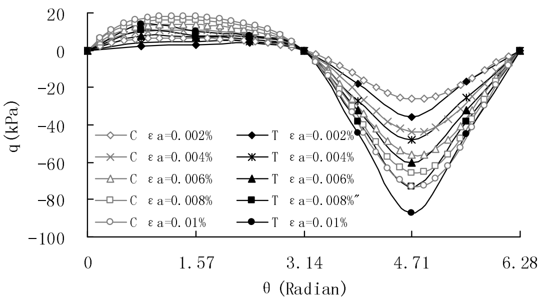

C: calculation, T: test

Figure 14 Relationship of the calculated and measured deviatoric

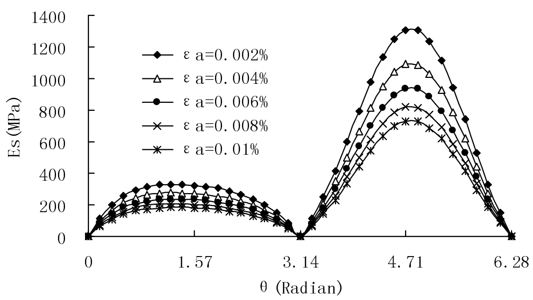

Figure 15 Effect of stress path direction on secant Young's modulus of elasticity

4. CONCLUSIONS

Through shear tests in the small strain region and the strain contour circle method for eight different triaxial stress paths for sands, the conclusions are as following:

1. The test results corresponding to eight stress paths are identical with the bounding surface of Wong-Mitchell, which indicates that the test results are credible. The inherent stress strain characteristics of soil are controlled by its anisotropic initial stress state, which has prominent difference from shear contraction and dilatation behaviour under isotropic initial stress condition.
2. The strain contour has similar circular shape under different strain values, the motion trace of contour center approaches a straight line. By using the proportion function λ and expansion function l, the strain contour circle method can consider all stress paths. The results are close to results of existing researches. The strain contour circle method can simulate small strain characteristics of stress path rationally.

5. ACKNOWLEDGEMENT

This research is financially supported by National Natural Science Foundation of China (No. 41172234). The authors are grateful to Professor Chui C F and Dr. Li J. H. for their suggestions.

6. REFERENCES

Atkinson, J. H., Richardson, D. & Stallebrass, S. E. (1990). "Effect of recent stress history on the stiffness of overconsolidated soil". Geotechnique 40, No. 4, pp531-540, doi: 10.1680/geot. 1990. 40.4.531.

Burland，J. B. (1989). "Small is beautiful –the stiffness of soils at small strains". Ninth Laurits Bjerrum memorial lecture. Canadian Geotechnical Journal 26, No. 4, pp499-514.

Charles, W. W. Ng, Pun, W. K. & Richard, P. L. P. (2000). "Small strain stiffness of natural granitic saprolite in Hong Kong". Journal of Geotechnical and Geoenvironmental Engineering 126, No.9, pp819-833.

Clayton, C. R. I. & Khatrush, A.(1989). "The use of Hall Effect semiconductors in geotechnical instrumentation". Geotech-nical Testing Journal 12, No. 1, pp69-76.

Clayton, C. R. I. (2011). "Stiffness at small strain: research and practice". Geotechnique 61, No. 1, pp5-37, doi: 10.1680 / geot. 2011. 61.1.5.

Clayton, C. R. I. & Heymann, G. (2001). "Stiffness of geomaterials at very small strains". Geotechnique 51, No. 3, pp245-255, doi: 10.1680/geot. 2001. 51.3.245.

Gasparre, A., Nishimura, S., Minh, N. A., Coop, M. R. & Jardine, R. J. (2007). "The stiffness of natural London Clay". Geotechnique, 57, No. 1, pp33–47, doi: 10.1680/ geot. 2007.57.1.33.

Goto, S., Burland, J. B. & Tatsuoka, F. (1999). "Non-linear soil model with various strain levels and its application to axisymmetric excavation problem". Japanese Geotechnical Society 39, No.4, pp111-119.

Hight, D. W., Gasparre, A., Nishimura, S., Minh, N. A., Jardine, R. J. & Coop, M. R. (2007). "Characteristics of the London Clay from the Terminal 5 site at Heathrow Airport". Geotechnique 57 ,No. 1, pp3–18, doi: 10.1680/geot. 2007. 57.1.3.

Jardine, R. J., Symes, M. J. & Burland, J. B. (1984). "The measurement of soil stiffness in the triaxial apparatus". Geotechnique 34, No. 3, pp323–340, doi: 10.1680/geot. 1984.34.3.323.

Jardine, R. J., Brooks, N. J. & Smith, P. R. (1985). "The use of electrolevel gauges intriaxial tests on weak rock". Inst. J. Rock Mech. Min. Sci. and Geomech. 22, No. 5, pp331-337.

Jardine, R. J. (1992). "Some observation on the kinematic nature of soil stiffness". Soils and Foundations 32, No. 2, pp111-124.

Kim, T and Finno, R. (2012). "Anisotropy evolution and irrecoverable deformation in triaxial stress probes". Journal of Geotechnical and Geoenvironmental Engineering 138, No.2, pp155-165. DOI: 10.1061 /(ASCE) GT.1943–5606 .0000575

Lai Yong, "Constitutive model considering stress path at small strain" [D], Hohai University, 2005.(in Chinese)

Lings, M. L., Pennington, D. S. & Nash, D. F. T. (2000). "Anisotropic stiffness parameters and their measurement in a stiff natural clay". Geotechnique 50, No. 2, pp109–125, doi: 10.1680/geot.2000.50.2.109.

Lo Presti, D. C. F., Jamiolkowski, M., Pallara, O., Cavallaro, A. & Pedroni, S. (1997). "Shear modulus and damping of soils". Geotechnique 47, No. 3, pp603-618, doi: 10.1680/geot. 1997.47.3.603.

Puzrin, A. M. & Burland, J. B. (1998). "Non-linear model of small-strain behavior of soils". Geotechnique 48, No.2, pp217-233, doi: 10.1680/geot.1998.48.2.217.

Shi, J. Y.，Lee, F. H. & Chong, P. T. (2001). "Research of constitutive model in anisotropic and small-strain condition (ASM) ". Geotechnical Engineering Journal 32, No.8, pp 83-90.

Shibuya, S., Tatsuoka, F., Teachavorasinskun, S. (1992). "Elastic deformation properties of geomaterials". Soils and Foundations 32, No.3, pp26-46.

Simpson, B. (1992). "Retaining structures: displacement and design". 32nd Rankine Lecture. Geotechnique 42, No. 4, pp541–576, doi:10.1680/geot.1992.42.4.541.

Smith, P. R., Jardine, R. J. & Hight, D. W. (1992). "The yielding of Bothkennar clay". Geotechnique 42, No.2, pp257-274, doi: 10.1680/geot.1992.42.2.257.

Stallebrass, S. E. & Taylor, R. N. (1997). "The development and evaluation of a constitutive model for the prediction of ground movement in overconsolidated clay". Geotechnique 47, No.2, pp235-253, doi: 10.1680/geot.1997.47.2.235.

Sultan, N. Cui, Y. J. and Delage, P. (2010) "Yielding and plastic behaviour of Boom clay". Geotechnique 60, No.9, pp657-666, doi: 10.1680/geot. 7.00142.

Thomann, T. G. & Hryciw, R. D. (1990). "Laboratory measurements of small strain shear modulus under K0 conditions". Geotech.Test. J. ASTM 13, No. 2, pp97–105.

Viggiani, G. & Atkinson, J. H. (1995). "Interpretation of bender element tests". Geotechnique 45, No. 1, pp149–154, doi: 10.1680/geot.1995.45.1.149.

Wong, P. K. K. and Mitchell, R. J., (1975) "Yielding and plastic flow of sensitive cemented clay". Geotechnique 25, No. 4, pp763-782., doi: 10.1680/geot.1975.25